Journal of the European Ceramic Society 20 (2000) 1043–1051

Effect of heat treatment on photoluminescence behavior of Zn_2SiO_4:Mn phosphors

Kee-Sun Sohn [a,*], Bonghyun Cho [a], Hee Dong Park [a], Yong Gyu Choi [b], Kyong Hon Kim [b]

[a] *Advanced Materials Division, Korea Research Institute of Chemical Technology, 100 Jangdong, Yuson-gu, Taejon 305-600, South Korea*
[b] *Telecommunication Basic Research Laboratory, Electronics and Telecommunications Research Institute, Daejon 305-350, South Korea*

Received 1 June 1999; received in revised form 30 August 1999; accepted 12 September 1999

Abstract

The thermal treatment in reducing atmospheres gives rise to the increase both in emission intensity and 10% decay time in Zn_2SiO_4:Mn phosphors. The present investigation aims to take account of such changes in association with the structural change. For this sake, X-ray absorption spectroscopy techniques such as XANES and EXAFS were conducted to the Zn_2SiO_4:Mn phosphors. The Zn_2SiO_4:Mn phosphors were fired in the air and then thermally treated in two different reducing atmospheres (hydrogen or carbon). The photoluminescent (PL) behavior was closely related to the X-ray absorption data. The XANES and EXAFS prove that the oxidation state (+2) remains identical regardless of whether or not the samples are treated, but that the Mn–O distance was reduced by the heat treatment. In order to give a plausible interpretation to the change in PL results, two possible suggestions are presented. Firstly, it is conceivable that the thermally activated diffusion process of manganese ions splits Mn–Mn pair during the heat treatment. Another possibility is that the thermal treatment annealed out some quenching site, which is related with defects and impurities. Such hypotheses can be rationalized systematically by considering the results from lifetime measurement, Debye–Waller factor calculation, and XANES pre-edge peaks.

Keywords: Phosphors; Photoluminescence; X-ray methods; Zn_2SiO_4–Mn

1. Introduction

The most significant qualification as a phosphor used for plasma display panel (PDP) requires high luminescent efficiency and appropriate decay time.[1] Zn_2SiO_4:Mn phosphors have been spotlighted as a green component in the PDP application. Considerable efforts have been made to fit the performance of Zn_2SiO_4:Mn phosphors to the PDP application.[2,3] They still need, however, a breakthrough to meet the requirements. First of all, the luminance should exceed 350 cd/m^2 and the life-time should be in the range between 1 and 5 ms. In order to attain a substantial advance, a theoretical approach has to precede so that one could get to the better understanding of photoluminescence (PL) behavior in this material. Many researchers have investigated the Zn_2SiO_4:Mn phosphors and developed an insight into the PL process of these materials. According to the earlier literatures,[4,5] the PL process of Zn_2SiO_4:Mn phosphors has been characterized by the transition of $3d^5$ electrons in the manganese ion acting as an activating center in the willemite structure. In particular, the transition from the lowest excited state to the ground state, i.e. $^4T_1(^4G)\rightarrow{}^6A_1(^6S)$ transition, is directly responsible for the green light emission. Some predecessors have investigated this transition and found that two different kinds of decay process are operating.[6,7] Such a difference is due to the different crystalline sites of zinc ions that manganese ion substitute for.[6] A more conspicuous feature is that some manganese ions make Mn–Mn pairs as the Mn concentration increases.[7] Barthou et al.[8] identified experimentally the decay process of both isolated Mn ions and Mn–Mn pairs by measuring the extremely high and low concentration of Mn. Based on the above findings, several research groups[2,8,9] have investigated these materials in terms of manganese doping content and developed some smart understandings both theoretically

* Corresponding author. Tel.: +82-42-860-7375; fax: +82-42-861-4245.
E-mail address: kssohn@pado.krict.re.kr (K.-S. Sohn).

0955-2219/00/$ - see front matter
PII: S0955-2219(99)00246-0

and experimentally. There is, however, still a need for a systematic understanding of the decay process in moderate Mn concentration regime (0.05∼0.12) in which favorable intensity and decay time are expected. On account of very complicated interactions between Mn ions, however, the decay behavior is too complicated to be interpreted with ease in this Mn concentration range.[8]

In the present investigation, the Zn_2SiO_4:Mn phosphors, which had experienced different processing procedures, were conducted to several experimental techniques such as emission and excitation spectra and decay measurement at both ambient and cryogenic (liquid N_2) temperatures. Some additional thermal treatments in different atmosphere resulted in different PL responses, which could be attributed to the structure change caused by the treatment. To investigate the structure-dependent PL process in a systematic manner, Mn K-edge XANES (X-ray absorption near edge structure) and EXAFS (extended X-ray absorption fine structure) were analyzed. These analyses provide some useful information about the oxidation state and short-range-order structure associated with Mn ions in the Zn_2SiO_4 lattice. A more accurate interpretation of PL process in Zn_2SiO_4:Mn phosphors could be achieved by combining both the X-ray absorption spectroscopy analyses and the results from the PL experiment. The primary interest is to investigate how the additional thermal treatment affects the structure and in turn the PL properties. In this regard, the present investigation will give another fine tuning to sort out the complications associated with the PL behavior of Zn_2SiO_4:Mn phosphors.

2. Experimental procedures

The materials used in the present investigation with the general formula $Zn_{2-x}Mn_xSiO_4$ have been prepared through the solid state reaction, for x values of 0.08 and 0.12. The raw materials used, ZnO, SiO_2, and MnO, are completely blended with a certain amount of acetone, dried, and fired at the temperature of 1300°C in the oxidizing (air) atmosphere (samples A0.08 and A0.12). For some phosphors (samples B0.08 and B0.12), the firing process is then followed by a reduction process at 900°C by introducing the gas mixture of nitrogen and a small amount of hydrogen (2%) into the furnace (reducing atmosphere), and thereby giving rise to higher emission intensity. On the other hand, a different reduction process is conducted to some other samples (sample C0.08 and C0.12) by using carbon atmosphere, that is, the mixture of phosphor powder and charcoal powder was fired in the inert atmosphere (nitrogen gas) at 1300°C. Such reduction processes enhance the emission intensity by about 50%. The reduced powders are pulverized and then examined using X-ray diffraction in order to check whether or not a single phase was obtained. The results confirm that the willemite structure (rhombohedral structure $\bar{R}3$) is certainly detected. All the powders even including the non-treated ones have a white body color, which indicates that all the manganese ions are in the divalent state.

As regards the PL measurement, the experimental skills adopted in the present investigation include emission and excitation spectra, and decay measurement, using a Perkin-Elmer LS50 spectrometer with a xenon flash lamp (the half width of a pulse is 10 μs). When the emission and excitation spectra were measured, the signals were gated for 20 ms, which is longer than the lifetime of the Zn_2SiO_4:Mn phosphors. On the other hand, the decay measurement was carried out with the gate time fixed at 20 μs by varying the delay time (0∼20 ms) after the cessation of a single pulsed irradiation. Such a process was repeated during the cycle time of 1 s and the signals were summed up to improve signal/noise ratio. In particular, a more precise decay measurement was performed separately during the very short period(< 1 ms) to detect the relatively fast decay in the early stage after the cessation of a single pulse.

X-ray absorption spectra in the photon energies of both below and above the Mn K-edge were recorded using a pair of Si (111) crystals at EXAFS Beamline BL3C1 of the Pohang Light Source (PLS). All spectra were measured in a transmission mode at room temperature. Energy was calibrated with a Mn metal foil within an energy resolution ($\Delta E/E$) estimated to be $\sim 10^{-4}$ at around the Mn K-edge. In each of the edge and EXAFS regions, data were recorded in steps of 0.1 eV and 0.01 Å^{-1}, respectively.

Mn K-edge XANES spectra of the samples and reference compounds were normalized with respect to the edge continuum jumps after a removal of the background. Final pre-edge absorption structure was obtained by subtracting the interpolated arc-tangent-fit to the main edge region of the XANES spectrum. On the other hand, background reduction, Fourier transforms into K- or R-space and non-linear least squares fit were done using the UWXAFS package.[10] Theoretical amplitude envelop and phase shift function of a Mn–O pair were calculated by FEFF6 code[11] and then calibrated using MnO and MnO_2 standard reference crystals. A detailed description on data reduction and fitting procedures can be found in the previous report.[12]

3. Results and discussion

Fig. 1(a) shows the emission spectra of the six samples under the 200 nm excitation, which shows that the reduction treatment promotes the maximum intensity of emission and also that the samples doped with Mn 0.12 mol are more efficient phosphors than those with Mn

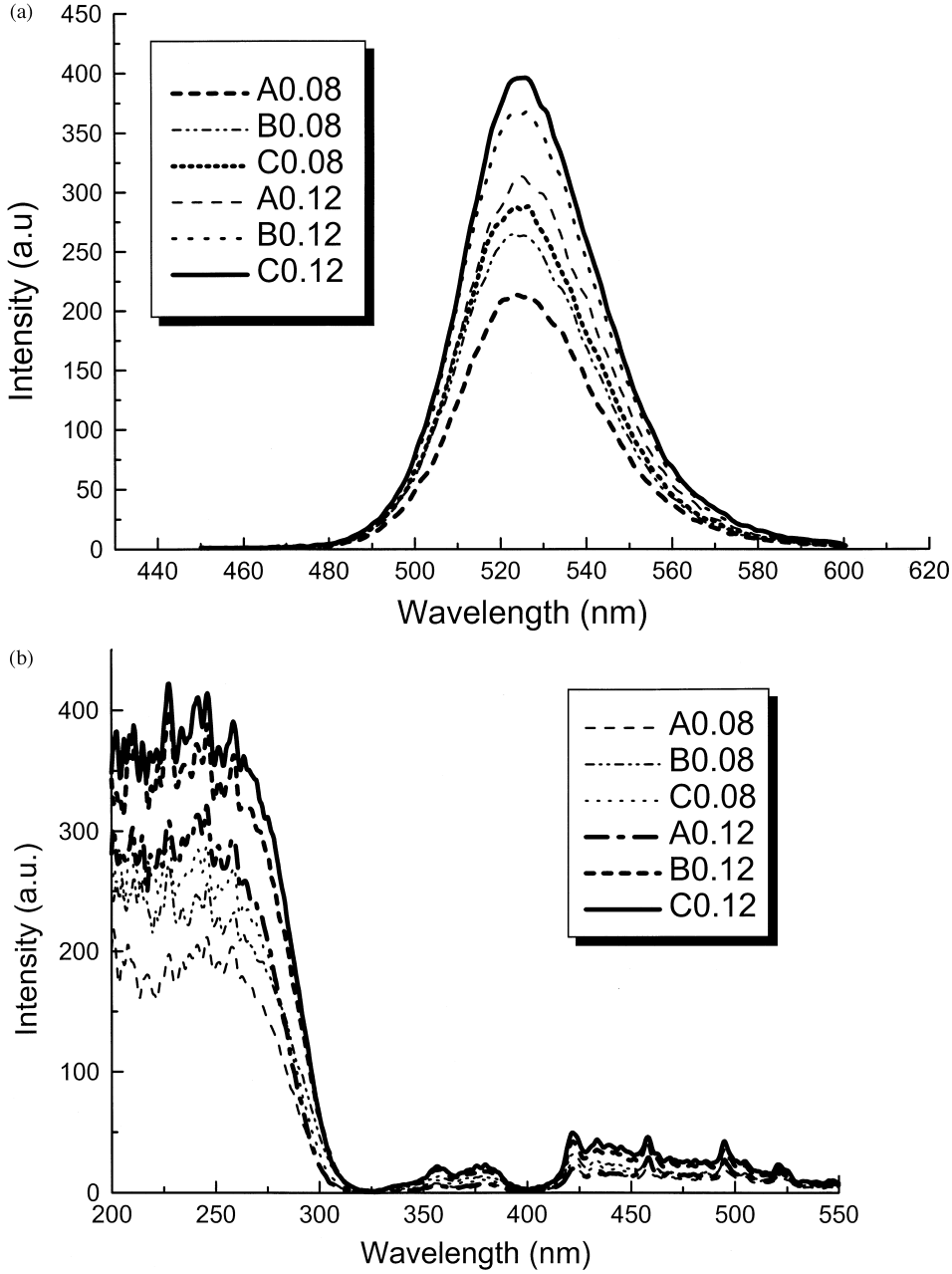

Fig. 1. Emission spectra (a) and excitation spectra (b) for both 0.08 and 0.12 Mn doped series. The capital letter A stands for firing at 1300°C in air without any further heat treatment, B refiring at 900°C in H_2 atmosphere, and C refiring at 1300°C in carbon atmosphere.

0.08 mol. Fig. 1(b) exhibits the excitation spectra of 524 nm emission for all the samples, the overall intensity level of which obeys the same order as observed in the emission spectra. That is, the carbon-reduced phosphor doped with 0.12 Mn shows the highest intensity. In particular, it should be noted that for both the Mn concentrations, the emission intensity of the phosphor treated using charcoal powder is slightly higher than the case of H_2 gas reduction. It may be ascribed to the effect of higher temperature.

Decay curves of 524 nm emission were measured under the UV excitation. Fig. 2 shows the 10% decay time at various excitation light wavelengths for both 0.08 and 0.12 series, respectively. As pointed out in the earlier literatures,[2,8,13] the higher Mn content, the shorter will be the decay time. Morell and Khiati[2] argued that such a behavior is closely related only with the concentration quenching. But more recently Barthou et al.[8] found that there exist two different activation centers of different decay time and that the faster color center is predominant at high Mn concentration, which is believed to be Mn–Mn pairs. Ronda and Amrein[14] suggested that the exchange interaction between Mn ions indeed results in allowed optical transitions on Mn ion

pairs and hence gives rise to shortening of decay time in relatively high Mn concentration. The 10% decay time of 0.12 Mn series, in fact, is estimated to be shorter than 0.08 Mn series by a factor of about 3 ms. Another interesting feature is that the treated samples (samples B and C) shows a much longer decay time than the non-treated ones (sample A).

On the other hand, the emission spectra of A0.08 and B0.08 were re-measured at 77°K in the same condition as the room temperature measurement. The results are presented in Fig. 3, showing the reduced half width of bands in comparison to the room temperature measurement and also a red shift of about 3 nm on going from A0.08 to B0.08. According to the Tanabe–Sugano diagram,[15] such a shift reflects the increase in crystal field. Marco de Lucas et al.[16] obtained a useful experimental results elucidating the dependence of emission band position on Mn–O distance for several manganese doped compounds that have a octahedrally coordinated Mn site. As a result, it turns out that the peak energy of

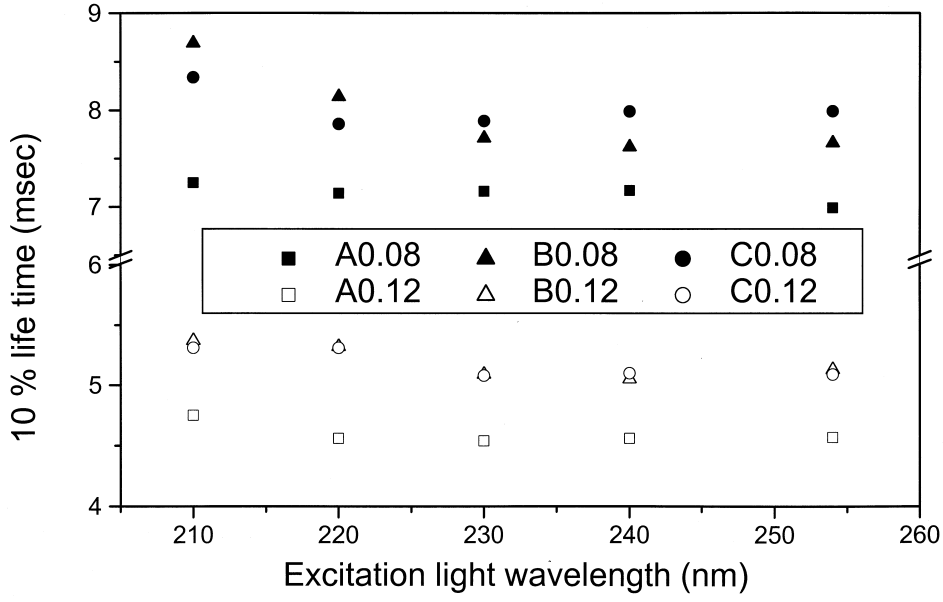

Fig. 2. 10% decay times under the various UV excitation wavelengths for both Mn 0.08 and 0.12 series. The capital letter A stands for firing at 1300°C in air without any further heat treatment, B refiring at 900°C in H_2 atmosphere, and C refiring at 1300°C in carbon atmosphere.

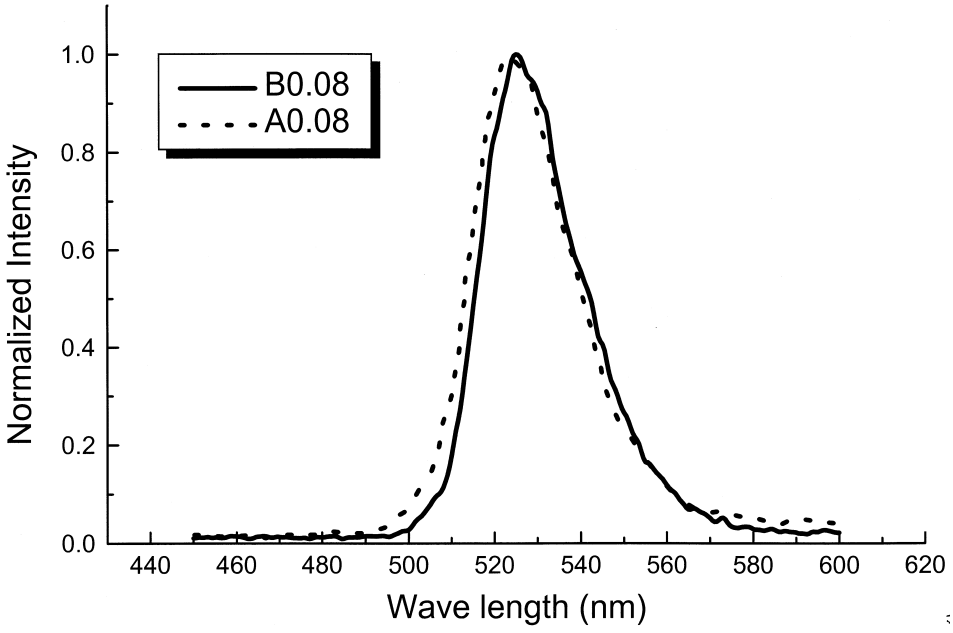

Fig. 3. Emission spectra obtained at 77 K for A0.08 and B0.08. The capital letter A stands for firing at 1300°C in air without any further heat treatment, and B refiring at 900°C in H_2 atmosphere.

manganese emission increases linearly with the Mn–O distance. The red shift observed in the present investigation should be due to the shortening of Mn–O distance in the heat-treated samples. In fact, such a shortening was reassured by the result from EXAFS analysis.

The main objective of this investigation is to find out the origin of the enhancement in emission intensity and decay time arising from the thermal treatment in the reducing atmosphere. According to some patents,[3,17] the reduction treatment has been considered to make some higher valent manganese ions reduced to +2 state, only in which Mn ions can emit the green light of interest. It is thus very important to know the exact oxidation state of manganese ions. In addition, the structural change of Zn_2SiO_4:Mn lattice may be induced by the reduction treatment, which eventually could give rise to the change in PL characteristics. X-ray absorption spectra such as XANES and EXAFS were measured to check all these things. For the convenience sake, only the A0.08, B0.08, and B0.12 samples were used for the XANES and EXAFS experiment.

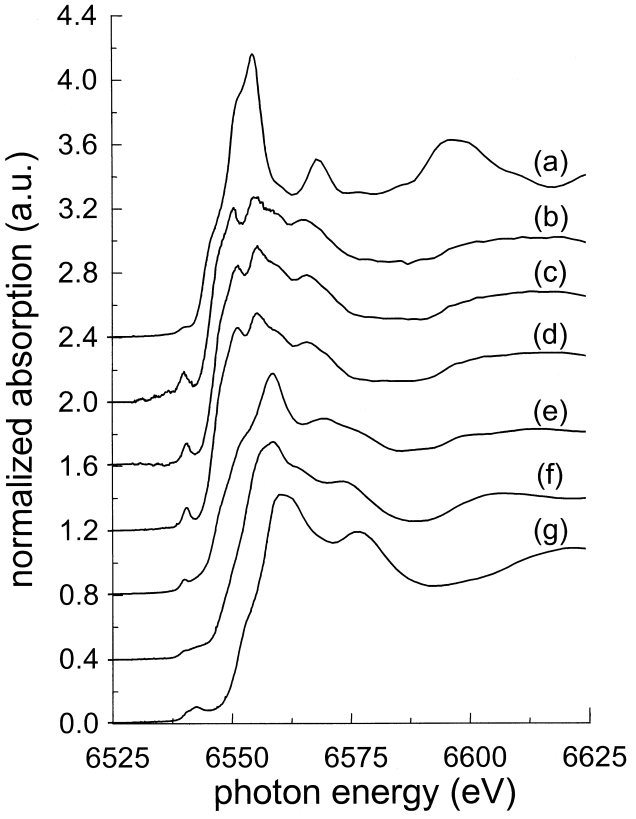

Fig. 4. Mn K-edge XANES spectra of reference and subject samples; (a) MnO, (b) sample A0.08, (c) sample B0.08, (d) sample B0.12, (e) Mn_3O_4, (f) Mn_2O_3, and (g) MnO_4.

The measured XANES spectra of the Mn doped Zn_2SiO_4 samples and various Mn reference compounds are presented in Fig. 4. The reference Mn compounds such as MnO, Mn_3O_4, Mn_2O_3, and MnO_2 were introduced for the systematic comparison with our samples. The main edge peak corresponding to the 1s→4p transition of the samples is split into two sub-peaks while no splitting takes place for the reference compounds. Relative intensity of the low-energy-side peak compared to the high-energy-side one in the edge crest of sample A0.08 [Fig. 4(b)] is larger than that of both samples B0.08 [Fig. 4(c)] and B0.12 [Fig. 4(d)]. Lineshape and intensity of the white lines of both the samples B0.08 and B0.12 are almost identical. The splitting in the vicinity of the edge crest is caused from a broken degeneracy in the antibonding orbitals due to asymmetrical metal–ligand bonding.[18] Therefore, the spectral splitting of the samples suggests that an asymmetry involved in Mn polyhedra of the sample A0.08 is bigger than that of the others. The main edge energy (E_o) determined as the most intense peak in the first derivative of XANES spectrum, shifts toward higher-energy side when the formal oxidation state of Mn ions in the reference compounds increases as shown in Table 1. However, it is known that the main-absorption-edge spectra are only rough measures of the Mn environment.[19] Nevertheless, the pre-edge peaks of the spectra correspond to the transition of 1s→3p which is possibly hybridized with the 3d states, and provide information on the oxidation state and oxygen coordination number of the samples. More specifically, the maximum energy (E_p) and full width at half maximum (W) of the pre-edge peak reflect the characteristics associated with the electronic and structural environment of the manganese. Final states with the 3d character associated with the preedge peak are more tightly bound and thereby less sensitive to changes in ionicity and long-range-order effects than the

Table 1
Measured spectroscopic and physical data of various Mn-containing reference oxide componds and Zn_2SiO_4 phosphor samples[a]

Material	MnO	Mn_3O_4	Mn_2O_3	MnO_2	A0.08	B0.08	B0.12
E_0 (eV)	6543.9	6546.8	6549.7	6551.3	6546.7	6546.7	6546.7
E_p (eV)	6540.0	–	6541.1	6542.4	6540.0	6540.5	6540.5
W (eV)	1.9	–	5.7	5.1	1.9	1.7	1.7
Oxygen co-ordination number	6	4,6	6	6	4	4	4
Oxidation site	2	2,3	3	4	2	2	2

[a] Main-edge energy (E_0), peak energy (E_p), full width at half maximum (W) of a pre-edge peak, oxygen co-ordination number in the nearest neighbour shell of Mn, and oxidation state of Mn in the hosts.

final states involved in the main edge are.[20] Thus, the oxidation state can be more easily determined from the energy position of the pre-edge peak. Our measured values of E_p for the samples coincide with that for the MnO reference, so that they confirm the +2 oxidation state of Mn for these phosphor samples. The measured peak intensities of the sample A0.08 and of the other two samples are about six times and five times larger than that of the MnO reference, respectively (Fig. 5). These behaviors can be explained by the fact that the ligand-field induced p–d mixing is symmetry dependent, and the absorption transition strength is governed by the centrosymmetry of the full point group. It is known that a low symmetry inherent in the tetrahedral environment leads to four to seven times intense preedge absorption peaks compared to that in the octahedral environment in general.[21] The current data indicate that the formation of MnO_4 tetrahedral unit may take place in the phosphor samples. The intense and broad absorption of the sample A0.08 compared with those of the samples B0.08 and B0.12 also proves that the Mn tetrahedra are more distorted in the sample A0.08.

Experimental Mn K-edge EXAFS interference functions of the samples shown in Fig. 6 have a nearly identical oscillation frequency up to photoelectron momentum value of ~ 9 Å^{-1}, which suggests that only the first nearest Mn–O shell is resolved in our spectra. This conjecture is confirmed from the observation of corresponding Fourier transform spectra shown in Fig. 7. Specifically, in these phase shift not corrected radial distribution function, a next nearest neighbor shell is not clearly observed. Its magnitude is, unfortunately, too small to deliver any meaningful information. Results obtained from a single-shell fit to the first Mn–O correlated peak are shown in Table 2. Oxygen coordination number of the samples is optimized to be 3.85∼3.97,

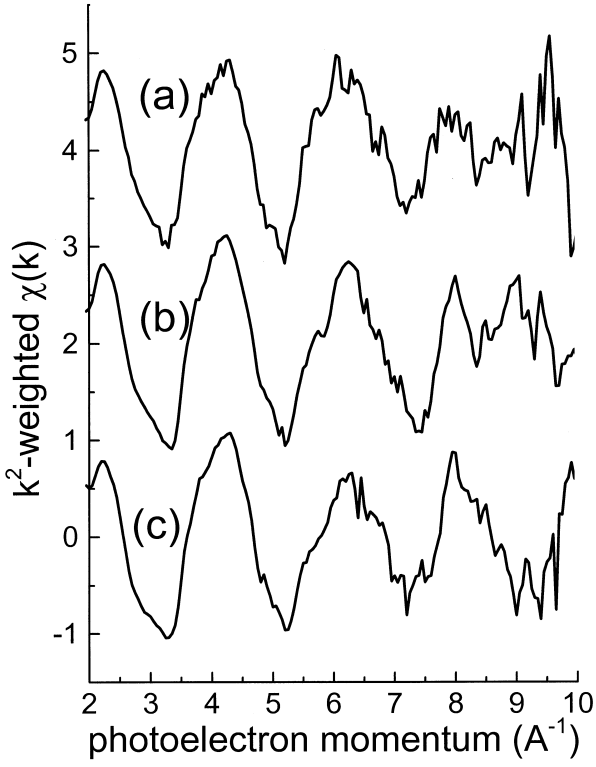

Fig. 6. Mn K-edge EXAFS spectra of (a) sample A0.08, (b) sample B0.08, and (c) sample B0.12.

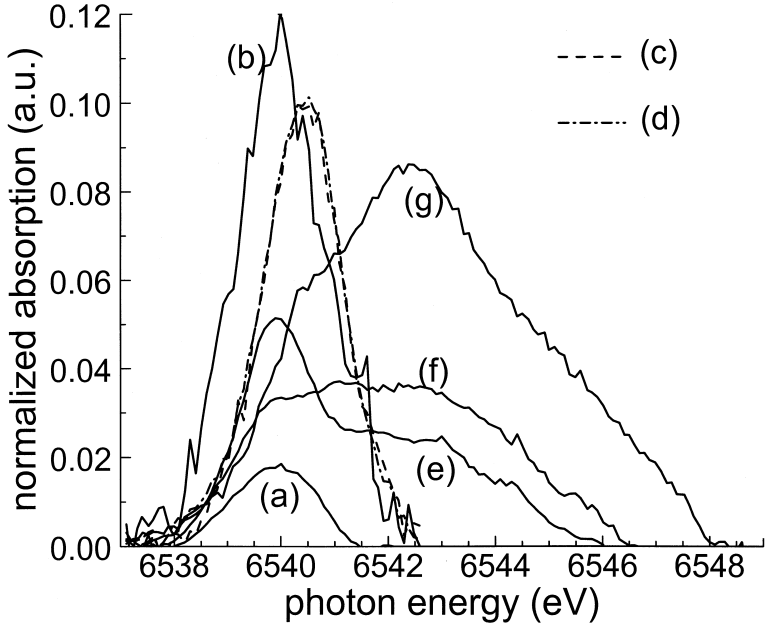

Fig. 5. Measured 1s→3p absorption peaks of reference and subject samples; (a) MnO, (b) sample A0.08, (c) sample B0.08, (d) sample B0.12, (e) Mn_3O_4, (f) Mn_2O_3, and (g) MnO_4.

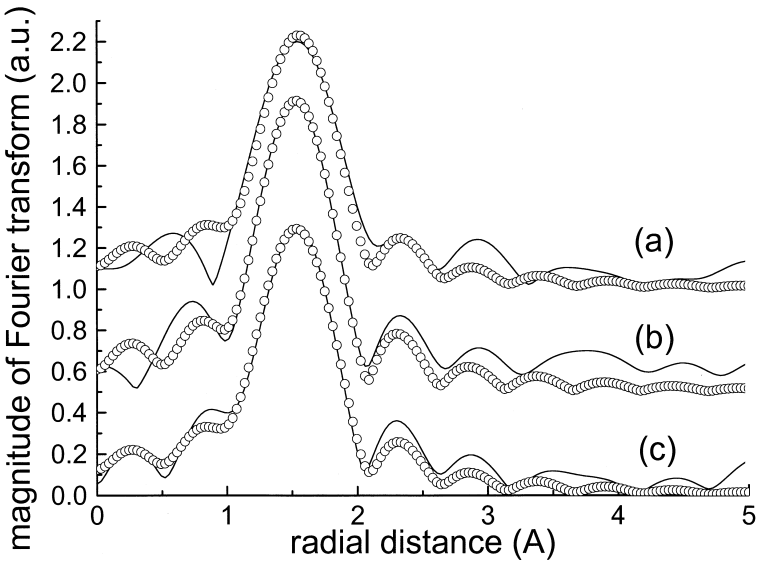

Fig. 7. Magnitude of Fourier transform of (a) sample A0.08, (b) sample B0.08, and (c) sample B0.12. Phase shift is not corrected. Solid line and circles represent the experimental and theoretical data, respectively.

Table 2
Fitting results on the nearest-neighbour peaks of Mn K-edge EXAFS of the $Zn_{2-x}Mn_xSiO_4$ samples[a]

Sample	Mn–O distance (A)	Co-ordination number	Debye–Waller factor (10^{-4} A^2)	R-factor[b]
A 0.08	2.046(0.010)	3.85(0.51)	47(25)	0.02
B 0.08	2.031(0.006)	3.93(0.32)	30(11)	0.005
C 0.12	2.033(0.006)	3.97(0.33)	26(13)	0.007

[a] Numbers in the parentheses are the estimated uncertainties.
[b] Calculated from the normalized difference between the experimental and theoretical values.

which suggests that a Mn ion is surrounded by four oxygen ions in the host. On the other hand, the EXAFS-type Debye–Waller factor associated with the Mn–O pairs is larger for the sample A0.08 than for the samples B0.08 and B0.12. The average Mn–O distance of the sample A0.08 (2.046 Å) is 0.01 Å longer than that of the samples B0.08 (2.031 Å) and B0.12 (2.033 Å). The bond length is closely related with valence of the bond, which can be calculated by using the bond-valence method.[22] The most common empirical expression being used to calculate the valence (ν_{ij}) of the bond with a length (R_{ij}) is

$$\nu_{ij} = \exp\left(\frac{B_{ij} - R_{ij}}{b}\right)$$

where B_{ij} is the bond valence parameter, and b is commonly taken as an universal constant (0.37 Å).[23] According to the above relationship, the calculated Mn–O bond length in a MnO_4 tetrahedron should be between 2.01 and 2.08 Å, provided that the oxidation number of Mn is 2 ($\pm$0.2) valence unit (VU). The Mn–O bond length determined in this study, therefore, coincides with the above estimation. An average Zn–O distance in the Zn_2SiO_4 crystal is approximately 1.96 Å[24] — the value obtained in the present investigation is almost identical to this value independent of whether or not the samples were heat treated. As a result, a certain degree of site swelling is inevitable when Mn dopes the crystal by taking into account the fact that the Mn^{2+} ion (0.66 Å) is bigger than the Zn^{2+} ion (0.60 Å) in the tetrahedral environment.[25]

We now need to discuss the correlation between the X-ray absorption data and the PL results. The most significant finding in the XANES and EXAFS data is that there is no change in Mn's oxidation state with respect to the thermal treatment. In view of conventional reduction, the reduction treatment could be expected to alter the oxidation state of constituent cations in the crystal, e.g. the electronic reduction of cations may occur (sometimes cations might be retrieved as a metallic form and even removed away) and constituent anions can also be eliminated by the reducing agent. It is unfortunate that only the change in oxidation state of the above-stated phenomena, is detectable in the XANES and EXAFS data. But although it is impossible to detect directly the removal of ions by the XANES and EXAFS, a considerable weight loss associated with the trace of Zn's volatilization could be actually observed during the experiment. Consequently, it is obvious from the XANES and

EXAFS data that the oxidation state of the Mn ions remains the same regardless of whether the reduction treatment is conducted or not. Hence, the enhancement in emission intensity and decay time, which is caused by the heat treatment, should not be interpreted by the change in Mn's oxidation state but by the other reduction effects. The result from the XANES and EXAFS implies that the reducing agent such as hydrogen gas and charcoal powder cannot play a decisive role to increase the number of Mn^{2+} ions during the treatment. In other words, there are very few Mn ions in higher valence states even in the non-treated samples. Actually, we confirmed that exactly the same improvement arose in the samples reheated in the neutral (N_2) atmosphere. Now that we could not observe Mn's valency change in the X-ray absorption data, an alternative interpretation should be given to the enhanced emission intensity and elongated decay time.

The structural changes caused by the heat treatment, such as the contraction of Mn–O distance, the relief from distortion, and etc., could not provide a direct evidence to account for the change in emission intensity and decay time. There is, however, no doubt that the structural changes observed around the Mn ions should be related to the change in PL behavior. One of the possible interpretations could be the defect impurity related hypothesis, i.e. the heat treatment could redistribute defect impurities and even eliminate some volatile impurities. Defect impurities are known to act as a quenching site in the host crystal. It is known that the existence of defect impurities acting as quenching sites deteriorates the PL property. The thermal removal of this kind of quenching site after the heat treatment could be the reason for the enhanced emission intensity and the elongated decay time. It is thus presumed that the heat treatment could restrain the non-radiative process by the elimination of impurities, so that the emission intensity as well as decay time could be promoted.

Another possible suggestion is that the thermally activated diffusion process of manganese ions increases the number of isolated Mn ions by splitting Mn–Mn pair during the heat treatment. The Mn–Mn pair, the number of which becomes larger when the Mn concentration increase, has been known to exhibit relatively fast decay[7,8] in comparison to the single Mn ion. The Mn concentration adopted in the present investigation is high enough to make a lot of Mn–Mn pairs, so that there could exist a large number of Mn–Mn pairs to be split by the heat treatment. This is why the heat treated samples show the more intense emission and longer decay. The distortion around the Mn–Mn pair may be quite considerable by taking into account the fact that the Mn^{2+} ion is larger than the Zn^{2+} ion. Such a disorder could be reckoned by referring to the Debye–Waller factor in the EXAFS data (see Table 2) and also to the height and width of pre-edge peaks. The Debye–Waller factor, which is indicative of static disorder,[26] decreases by more than 50% on going from non-treated to treated samples. The more intense and broader pre-edge peak as well as more prominent splitting of main edge peak in A0.08 compared to B0.08 and B0.12 also indicates that the Mn tetrahedra are more distorted in the sample A0.08. Moreover, the volatilization of Zn ions may provide some vacancies, which could facilitate Mn diffusion. In this context, one can suggest that the heat treatment splits the Mn–Mn pairs. In doing so, the change in Debye–Waller factor and pre-edge peak could be rationalized in a systematic manner and hence the longer decay time and higher PL intensity also make sense.

4. Conclusions

1. It is found from a Mn K-edge XAS that the most Mn ions are in four-fold co-ordination of oxygen and in $+2$ valency state in the Zn_2SiO_4 host. The average Mn–O distance in as-synthesized sample is measured to be $\sim$2.04 Å and found to decrease by $\sim$0.01 Å after the additional thermal treatment in the reducing atmospheres. Moreover, a structural disorder associated with the oxygen arrangement around the Mn becomes low after the heat treatment.
2. It is revealed that there is no drastic change in Mn's oxidation state after the heat treatment. Besides Mn's valency change, some other effects should be considered to explain the enhanced PL property caused by the heat treatment. Either the removal of some impurity ions or the Mn–Mn pair splitting could be possible hypotheses, which can give a reasonable explanation as regards to the increase in emission intensity and decay time caused by the heat treatment.

Acknowledgements

The authors wish to thank Dr. Jay Min Lee at Pohang accelerator laboratory in Pohang University of Science and Technology for his arrangement for X-ray absorption measurement at Pohang Light Source (PLS), which were financially supported in part by MOST and POSCO.

References

1. Koike, J., Present and future prospects of phosphors for plasma display. In Extended Abstracts of the Third International Conference on the Science & Technology of Display Phosphors, Huntington Beach, CA, 3–5 November 1997, pp. 13–16.
2. Morell, A. and Khiati, N.El, Green phosphors for large plasma TV screens. *J. Electrochem. Soc.*, 1993, **140**, 2019–2022.

3. Morell, A. and Goumard, N., Phosphor material based on manganese-doped zinc silicate and method for obtaining such a material. United States Patent 5645761, 8 July 1997.
4. Perkins, H. K. and Sienko, M. J., ESR study of manganese-doped zinc silicate crystal. *J. Chem. Phys.*, 1967, **46**, 2398–2401.
5. Palumbo, D. T. and Brown, J. J. Jr., Electronic states of Mn^{2+}-activated phosphors. *J. Electrochem. Soc.*, 1970, **117**, 1184–1188.
6. Stevels, A. L. N. and Vink, A. T., Fine structure in the low temperature luminescence of Zn_2SiO_4:Mn and $Mg_4Ta_2O_9$:Mn. *J. Lumin.*, 1974, **8**, 443–451.
7. Robbins, D. J., Mendez, E. E., Giess, E. A. and Chang, I. F., Pairing effects in the luminescence spectrum of Zn_2SiO_4:Mn. *J. Electrochem. Soc.*, 1984, **131**, 141–146.
8. Barthou, C., Benoit, J., Benalloul, P. and Morell, A., Mn^{2+} concentration effect on the optical properties of Zn_2SiO_4:Mn phosphors. *J. Electrochem. Soc.*, 1994, **141**, 524–528.
9. Chang, I. F., Brownlow, J. W., Sun, T. I. and Wilson, J. S., Refinement of zinc silicate phosphor synthesis. *J. Electrochem. Soc.*, 1989, **136**, 3532–3536.
10. Stern, E.A, Newville, M., Ravel, B., Yacoby, Y. and Haskel, D., The UWXAFS analysis package: philosophy and details. *Physica B*, 1995, **209**, 117–120.
11. Rehr, J. J., Mustre de Leon, J., Zabinsky, S. I. and Albers, R. C., Theoretical X-ray absorption fine structure standards. *J. Am. Chem. Soc.*, 1991, **113**, 5135–5140.
12. Choi, Y. G., Heo, J. and Chernov, V. A., Ga K-edge EXAFS analyses on the coordination of gallium in $PbO–Ga_2O_3$ glasses. *J. Non-Cryst. Solids*, 1997, **221**, 199–207.
13. Chang, I. F. and Sai-Halasz, G. A., Investigation of energy traps and phosphorescence in zinc silicate phosphors by photostimulated emission. *J. Electrochem. Soc.*, 1980, **127**, 2458–2464.
14. Ronda, C. R. and Amrein, T., Evidence for exchange-induced luminescence in Zn_2SiO_4:Mn. *J. Lumin.*, 1996, **69**, 245–248.
15. Blasse, G. and Grabmaier, B. C., *Luminescent Materials*. Springer–Verlag, 1994, pp. 20–25.
16. Marco de Lucas, M. C., Rodriguez, F. and Moreno, M., Zero-phonon transition and the Stokes shift of Mn^{2+}-doped perovskites: dependence on the metal–ligand distance. *Phys. Rev.*, 1994, **50**, 2760–2765.
17. Chenot, C. F. and Minnier, H. B., Method for preparing zinc orthosilicate phosphor. United States Patent 5188763, 23 February 1993.
18. Apte, M. Y. and Mande, C. J., The shape and extended fine structure of the manganese K X-ray absorption discontinuity in its oxides. *Phys. Chem. Solids*, 1980, **41**, 307–312.
19. Belli, M., Scafati, A., Bianconi, A., Mobilio, S., Palladino, L., Reale, A. and Burattini, E., X-ray absorption near edge structures (XANES) in simple and complex Mn compounds. *Solid State Comm.*, 1980, **35**, 355–361.
20. Manceau, A., Gorshkov, A. I. and Drits, V. A., Structural chemistry of Mn, Fe, Co, and Ni in manganese hydrous oxides: part I. Information from XANES spectroscopy. *American Mineralogist*, 1992, **77**, 1133–1143.
21. Lytle, F. W., Greegor, R. B. and Panson, A. J., Discussion on X-ray absorption near edge structure: application to Cu in high T_c superconductors, $La_{1.8}Sr_{0.2}CuO_4$ and $YBa_2Cu_3O_7$. *Phys. Rev. B*, 1988, **37**, 1550–1562.
22. Brese, N. E. and O'Keeffe, M., Bond-valence parameters for solids. *Acta Cryst.*, 1991, **B47**, 192–197.
23. Brown, I. D. and Altermatt, D., Bond-valence parameters obtained from a systematic analysis of the inorganic crystal structure database. *Acta Cryst.*, 1985, **B41**, 244–247.
24. Calculated from the ATOMS code.
25. Shannon, R. D., Revised effective radii and systematic studies of interatomic distances in halides and chalcogenides. *Acta Cryst.*, 1976, **A32**, 751–767.
26. Teo, B. K., EXAFS: *Basic Principles & Data Analysis*. Springer–Verlag, 1986, pp. 24–31.